The structure of Er^{3+}-doped oxy-fluoride transparent glass-ceramics studied by Raman scattering

EUROPHYSICS LETTERS 15 November 2003

Europhys. Lett., **64** (4), pp. 529–535 (2003)

The structure of Er^{3+}-doped oxy-fluoride transparent glass-ceramics studied by Raman scattering

V. K. Tikhomirov[1], A. B. Seddon[1], M. Ferrari[2], M. Montagna[3], L. F. Santos[4] and R. M. Almeida[4]

[1] *Novel Photonic Glasses Research Group, Centre for Advanced Materials University of Nottingham - Nottingham NG7 2RD, UK*
[2] *CNR-IFN, Istituto di Fotonica e Nanotecnologie - 38050 Povo (TN), Italy*
[3] *INFM, Dipartimento di Fisica, Università di Trento - 38050 Povo (TN), Italy*
[4] *Departamento de Engenharia de Materiais / INESC-ID, Instituto Superior Técnico Av. Rovisco Pais, 1049-001 Lisboa, Portugal*

(received 19 August 2002; accepted in final form 9 September 2003)

PACS. 81.05.Pj – Glass-based composites, vitroceramics.
PACS. 61.46.+w – Nanoscale materials: clusters, nanoparticles, nanotubes, and nanocrystals.
PACS. 78.30.Ly – Disordered solids.

Abstract. – We show that the structure of transparent oxy-fluoride glass-ceramics formed by heat treatment of glasses of typical composition $32(SiO_2)$:$9(AlO_{1.5})$:$31.5(CdF_2)$:$18.5(PbF_2)$:$5.5(ZnF_2)$:$3.5(ErF_3)$ mol% consists of $\sim$ 12 nm diameter, Er^{3+}-doped, β-PbF_2 nano-crystals embedded in a silica-based glass network and connected to it via non-bridging O and F anions, or fluorine linkages such as Pb-F-Cd and Pb-F-Zn. It is proposed that the glass network structure is mostly chain-like and dominated by $Si(O,F)_4$ tetrahedra with two bridging O and two non-bridging O and/or F atoms (Q^2 units). SiO_4 tetrahedra with zero and one bridging O (Q^0 and Q^1 units, respectively) are also present in the glass structure, in the approximate proportion $Q^0 : Q^1 : Q^2 = 1 : 1 : 3$, a characteristic which appears to be of primary importance. The flexible, chain-like glass-network, with many broken bonds, results in easy accommodation of the Er^{3+}-doped PbF_2 nano-crystals, which are grown by heat-treatment of the precursor glass. The boson peak in the Raman spectrum of the precursor glass decreases in intensity upon ceramming and is partly converted to narrow crystalline peaks at lower frequency, consistent with the precipitation of PbF_2 crystalline nano-particles. It is suggested that the boson peak involves localized vibrations of broken or stretched Pb-F bonds. The mean free path for these vibrations increases with ceramming, which involves partial crystallization of the glass network, resulting in a shift of the boson peak vibrations to lower-frequency crystalline peaks.

We have shown recently [1,2] that Er^{3+}-doped ultra-transparent glass-ceramics (GC) can be prepared in the oxy-fluoride system $(SiO_2)(Al_2O_3)(CdF_2)(PbF_2)(ZnF_2)$: $x(ErF_3)$. On heat-treating, Er^{3+} nucleates the growth of nano-crystalline β-PbF_2, which acts as its host. The typical size of the spherical nano-crystals is $\sim$ 1 to 12 nm depending on the parameters of heat-treatment [2]. These GC exhibit the broadest and flattest emission band of Er^{3+} dopant in the 1.54 μm telecommunications window ($^4I_{13/2} \rightarrow {}^4I_{15/2}$ transition) reported to date [1,2].

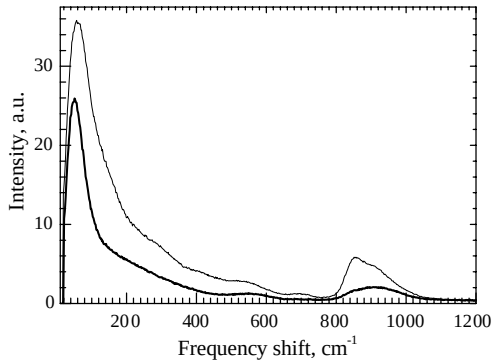

Fig. 1 – Raman scattering spectra of the base glass $32SiO_2$:$9AlO_{1.5}$:$31.5CdF_2$:$18.5PbF_2$:$5.5ZnF_2$: $3.5ErF_3$, in the polarized (VV, thin line) and depolarized (HV, thick line) configurations.

In this paper, we report a Raman scattering study of the respective precursor oxy-fluoride glasses and resulting GC with the overall aim of elucidation of the structure of GC. Polarized Raman measurements at low frequency show two narrow crystal-like peaks at 3.6 and 7.7 cm^{-1} in the GC, which were absent in the precursor glass. These features are due to quadrupolar and symmetric spherical acoustic vibrations, respectively, localized on the spherical nano-crystals of β-PbF_2. The fact that scattering peaks can be detected at such low frequencies is indicative of a very weak Rayleigh scattering wing in these, therefore, ultra-transparent GC. On the other hand, a very intense boson peak was observed at about 75 cm^{-1}, and its intensity and width decreased with ceramming of the precursor glass simultaneously with the appearance of the afore-mentioned crystalline peaks. We shall discuss the mechanism of conversion of the boson peak into crystal-like peaks.

The high-frequency Raman scattering region, on the other hand, indicated the presence of vibrations in structural units of the Q^n-type ($0 < n < 2$), which correspond to $\mathrm{Si(O,F)}_4$ tetrahedra with n bridging oxygens, interconnected via Si-O-Al and Si-O-Si bridges. To our knowledge, this is a first observation of $Q^{(n)}$-type ($0 < n < 2$) units in the structure of the oxy-fluoride precursor glass and resulting glass-ceramics. The optimum ratio between the $Q^{(n)}$ units was found to be about $Q^0 : Q^1 : Q^2 = 1 : 1 : 3$, which allowed easier incorporation of β-PbF_2 nano-crystals into the precursor glass network as will be discussed later. The PbF_2 nano-crystals appear to be bonded into this alumino-silicate glass network via non-bridging O and F anions (belonging to the Q^0, $Q^{(1)}$, $Q^{(2)}$ units), or fluorine (*e.g.*, Pb-F-Cd, Pb-F-Zn) linkages, as indicated by the bending vibration peaks at 160–500 cm^{-1}.

The procedures for preparation of undoped and Er^{3+}-doped precursor glasses and resulting ultra-transparent GCs are described in [2]. Non-resonant excitation of Raman scattering was carried out using the 457 nm line of Ar laser, at which there are neither Er^{3+} absorption bands, nor the electronic absorption edge of the glasses and resulting GCs. Scattered light was collected at 90° relative to the excitation beam, in the HH or VV (polarized) and HV (depolarized) configurations [3].

Figure 1 shows the polarized Raman spectra of the precursor glass, or base glass $32SiO_2$: $9AlO_{1.5}$:$31.5CdF_2$:$18.5PbF_2$:$5.5ZnF_2$: $3.5ErF_3$ mol%. The measured intensity $I(\omega)$ is defined from eq. (1) [4]:

$$I(\omega) = c(\omega)\frac{g(\omega)[n(\omega)-1]}{\omega}\,, \tag{1}$$

where $g(\omega)$ is the density of vibrational states; $n(\omega)+1$ is the Bose-Einstein thermal population

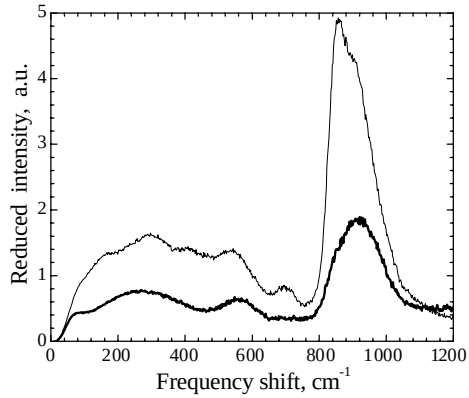

Fig. 2 – Reduced Raman scattering spectra of the base glass $32SiO_2$:$9AlO_{1.5}$:$31.5CdF_2$: $18.5PbF_2$:$5.5ZnF_2$: $3.5ErF_3$, in the polarized (VV, thin line) and depolarized (HV, thick line) configurations.

factor, and $c(\omega)$ is the Raman coupling coefficient. Due to the thermal population factor, the measured spectra at $\omega \leq 300\,\mathrm{cm}^{-1}$, do not properly represent the density of vibrational states. Therefore, we plot in fig. 2 the reduced Raman spectra, $I_{\mathrm{R}}(\omega)$, corresponding to measured spectra of fig. 1. $I_{\mathrm{R}}(\omega)$ is defined by eq. (2):

$$I_{\mathrm{R}}(\omega) = I(\omega)\frac{\omega}{n(\omega)+1} = c(\omega)g(\omega). \tag{2}$$

$I_{\mathrm{R}}(\omega)$ is an adequate representation of the density of vibrational states, $g(\omega)$, because $c(\omega)$ is approximately constant for each vibrational mode.

Figure 3 shows the expanded very low-frequency Stokes and anti-Stokes parts of Raman spectra for the base glass and resulting GC in polarized VV configuration.

Based on figs. 1, 2 and 3, we identify four series of scattering peaks, whose origin is further discussed below. The band between 750 to $1100\,\mathrm{cm}^{-1}$ corresponds to vibrations of the $Q^{(0)}$, $Q^{(1)}$, $Q^{(2)}$ units (see [5] and references therein) in the alumino-silicate glass network. The band

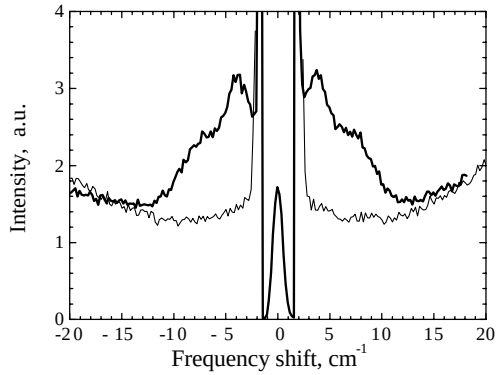

Fig. 3 – Ultra-low–frequency Stokes and anti-Stokes Raman scattering spectra of the base glass $32SiO_2$:$9AlO_{1.5}$:$31.5CdF_2$:$18.5PbF_2$:$5.5ZnF_2$: $3.5ErF_3$ (thin line) and resulting glass-ceramics (thick line) in the polarized VV configuration.

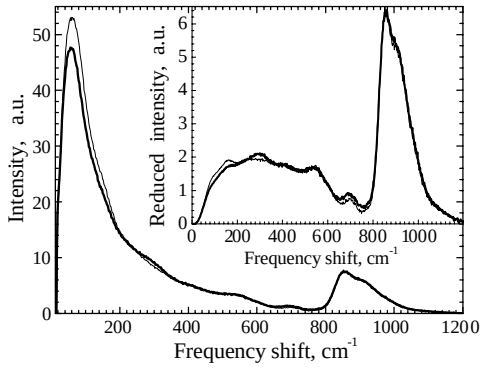

Fig. 4 – Raman scattering spectra of the base glass $32SiO_2$:$9AlO_{1.5}$:$31.5CdF_2$:$18.5PbF_2$:$5.5ZnF_2$:$3.5ErF_3$ (thin line) and resulting glass-ceramics (thick line) in the polarized (VV) configuration. The insert are the same spectra, after reduction.

at $700\,\mathrm{cm}^{-1}$ is due to bending vibrations in Si-O-Si bridges [5], while the band at $545\,\mathrm{cm}^{-1}$ may be due to vibrations of Al-O-Al bridges [5]. The latter band, essentially depolarized, may also involve asymmetric stretching vibrations of (Zn, Cd, Pb)-F-(Zn, Cd, Pb) bridges, based on the range of Raman frequencies observed in fluoride glasses containing Zn and Cd [6]. The bands at 160, 290 and $410\,\mathrm{cm}^{-1}$ are due to bending vibrations of (Zn, Cd, Pb)-F-(Zn, Cd, Pb) fluoride bridges, such as Cd-F-Pb or Cd-F-Zn, similar to the bands of purely fluoride glasses based on ZnF_2-CdF_2 [6], or ZrF_4-PbF_2 and HfF_4-PbF_2 binary glasses [3, 7]. Finally, the boson peak, at $75\,\mathrm{cm}^{-1}$ in the measured spectra, and at $50\,\mathrm{cm}^{-1}$ in the reduced spectra, is observed. It is accompanied by narrow peaks at 3.6 and $7.7\,\mathrm{cm}^{-1}$ (see fig. 3, thick line) which correspond to vibrations of crystalline nano-particles [8, 9]. These peaks were absent from the spectra of the corresponding base glass (see fig. 3, thin line). Weak luminescence of the host glass may slightly affect the Raman bands at 260 and $560\,\mathrm{cm}^{-1}$, as well.

Figure 4 shows the difference between the Raman spectra of the base glass and the resulting GC. Apart from the crystalline peaks at 3.6 and $7.7\,\mathrm{cm}^{-1}$, already mentioned (fig. 3), the difference is that the boson peak decreases in intensity for the GC, compared to the base glass. A small change is also seen in the reduced intensity (insert in fig. 4) of bands at 160, 290 and $700\,\mathrm{cm}^{-1}$, which correspond to bending vibrations of fluoride and oxide bridges. This indicates changes in polarizability/length of those bridges on ceramming. No difference between the Raman spectra of the base glass and resulting GC is seen for the band between 750 and $1100\,\mathrm{cm}^{-1}$, which corresponds to vibrations of the Q^0, $Q^{(1)}$, $Q^{(2)}$ units.

Figure 5 shows deconvolution into three Gaussian bands of that part of the Raman spectrum, which corresponds to $Q^{(n)}$-type vibrations of $Si(O, F)_4$ tetrahedra. The deconvolution is valid for both the precursor glass and resulting glass-ceramics, as no difference in their Raman spectra is detected in the range 750 to $1100\,\mathrm{cm}^{-1}$ (see fig. 4). Their assignment is given below. Origin 7.0 software was used for the deconvolution. Deconvolution either in two or four Gaussian bands was found to be essentially impossible.

We now suggest a structural interpretation of the observed Raman spectra. Crystal-like peaks, being absent in the precursor glass (fig. 3), indicate nano-particles in the GC, grown on heat treatment of the precursor glass. X-ray diffraction (XRD) and transmission electron microscopy (TEM) studies demonstrated the presence of 12 nm diameter crystalline particles in these GC [2], while a simultaneous energy dispersive analysis (EDS) showed that the nano-particles composition is PbF_2 [10]. Specifically, these nano-particles are in an Er^{3+}-doped

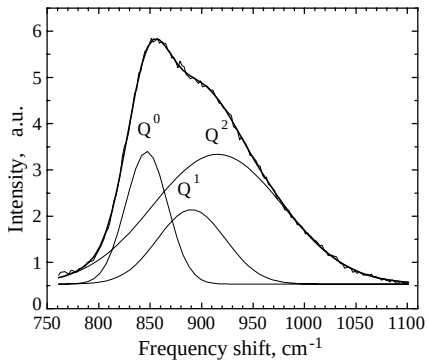

Fig. 5 – Deconvolution of the region of the polarized (VV) Raman scattering spectrum of the base glass $32SiO_2$:$9AlO_{1.5}$:$31.5CdF_2$:$18.5PbF_2$:$5.5ZnF_2$: $3.5ErF_3$ and/or resulting glass-ceramics, which corresponds to $Q^{(n)}$-type vibrations in the silicate glass network. The noisy curve is the measured spectrum and the thick solid line is the resulting fit. The three components $Q^{(0)}$, $Q^{(1)}$ and $Q^{(2)}$ are represented by Gaussian peaks (thin lines).

β-PbF_2 phase, which is created following the $\alpha \rightarrow \beta$ phase transition of PbF_2 once nucleated by Er^{3+} upon heat treatment of the precursor glass [2].

Theory [8,9] gives the typical size and size distribution for nano-particles embedded in the glass-network, based on frequency ω and linewidth of crystal-like peaks. The low-frequency VV spectrum for GC in fig. 3, after subtracting background, is a good fit with Gaussian peaks centred at $\omega_2 = 3.6\,\mathrm{cm}^{-1}$ and $\omega_0 = 7.7\,\mathrm{cm}^{-1}$ with linewidths $4.4\,\mathrm{cm}^{-1}$ and $3.5\,\mathrm{cm}^{-1}$, respectively. The subscript stands for quadrupolar ($\ell = 2$) and symmetric spherical ($\ell = 0$) surface acoustic vibrations [8,9]. The HV spectrum of the GC (see fig. 4 in [2]) has only a vibration at $\omega_2 = 3.6\,\mathrm{cm}^{-1}$, at the same frequency as in the VV polarization. In a free sphere approximation, the frequencies ω_0, ω_2 are given by eq. (3):

$$\omega_j = \frac{S_j \nu_j}{dc}\,, \tag{3}$$

where S_0 and S_2 are defined by the ratio of longitudinal $\nu_0 = \nu_\mathrm{L} = 3470\,\mathrm{m/s}$ and transversal $\nu_2 = \nu_\mathrm{T} = 1730\,\mathrm{m/s}$ sound velocities in β-PbF_2 [11], d is the diameter of nano-particle, and c is the light velocity. As the ratio $\nu_\mathrm{L}/\nu_\mathrm{T} \sim 2$, we have after [8,9] $S_0 = 0.87$ and $S_2 = 0.84$, that is $S_0\nu_\mathrm{L}/S_2\nu_\mathrm{T} = 2.07$. This ratio agrees well with the experimentally observed ratio $\omega_0/\omega_2 = 2.1$. The diameter of nano-particles, calculated from eq. (3) is then 13 nm, in good agreement with the value 12 nm obtained from XRD and TEM studies [2]. This proves that the theory of acoustic vibrations in nano-particles [8,9] can be applied to nano-scale glass-ceramics.

Homogeneous broadening of linewidths due to interaction of nano-particle spheres with surrounding glass network and inhomogeneous broadening due to their size distribution will be taken into account in further detailed studies. For this one needs the sound velocity of the surrounding glass, but that is speculative at present. However, the inhomogeneous broadening results in an overestimated value for the diameter of nano-particles [8,9]. Since the value 13 nm deduced from the Raman spectrum is very close to the value 12 nm deduced from XRD and TEM studies, we actually assert that the inhomogeneous broadening is not so important and the size distribution of the nano-particles is not wide.

The appearance of crystal-like peaks in GC (fig. 3) occurs simultaneously with a decrease of the boson peak with ceramming (fig. 4). An analogous effect was reported in the case of magnesium aluminosilicate glass-ceramics [12], indicating that this effect is quite general. Thus,

the vibrations, which give rise to the boson peak (mostly of optical origin [13]), partly convert into the acoustic vibrations responsible for crystal-like peaks [8,9]. As the nano-crystals are β-PbF_2, *i.e.* a fluoride within an oxide matrix, the boson peak will involve scattering on broken/stretched bonds [14], Pb-F in this case, which produce fluctuations of polarizability that account for this peak. Precipitation of PbF_2-enriched areas as a crystalline phase in GC results in a certain degree of long-range order and hence delocalization of previously localized vibrations and in an increase of the mean free path of the latter, leading to a shift to lower frequency, producing narrow crystal-like peaks (fig. 3).

The spectral deconvolution shown in fig. 5 indicates that $Q^{(n)}$-type ($n = 0, 1, 2$) units [5] are present, with the ratio between the corresponding areas of $Q^0 : Q^1 : Q^2 = 1 : 1 : 3$. When the chemical composition was slightly changed, *e.g.* when the $SiO_2/AlO_{1.5}$ ratio was varied, the proportion of the different Q units was changed, with a reduction of $Q^{(0)}$ units and spherical nano-particles did not precipitate. Therefore, $Q^{(0)}$ units are most probably located near the boundaries of the nano-particles in the base composition. This is reasonable, since such units have no bridging O species and, therefore, they should tend to release the stress at the interface between the crystalline and glassy phases. $Q^{(1)}$ and $Q^{(2)}$ units, having one and two bridging O, respectively, built the chain-like glass-network, whose flexibility helps to accommodate the crystalline nano-particles of substantially different molar volume.

The frequencies for $Q^{(0)}$ and $Q^{(1)}$ units in fig. 5 are in excellent agreement with values given in the thorough review of McMillan on silicate glasses [5]. Therefore, we ascribe them as SiO_4 tetrahedra with zero and one bridging O, respectively. The frequency of the $Q^{(2)}$ units in fig. 5 (at $920\,cm^{-1}$) is remarkably lower than in [5] (at 950–$1000\,cm^{-1}$), this could be due to the substitution of some of the F for O. The reason why the frequency becomes lower when F replaces O is that F forms only one bond, while O may form two bonds, which are therefore stronger, with higher force constant. $Q^{(2)}$ then could be $Si(O,F)_4$ tetrahedra, with two bridging O, and two non-bridging O and/or F.

The spectra of figs. 1 and 2 indicate the presence of fluoride bridging units, such as Pb-F-Cd, Cd-F-Zn. They may be important intermediates in the glass-network structure, still preserving its chain-like, two-dimensional structure. They could also be at the boundary between crystalline nano-particles and the glassy matrix.

It is worth noting that ceramming results in some change of polarizability of fluoride bridges (like Pb-Cd-F) and oxide (such as Si-O-Si), as indicated by the slight difference in intensity of the corresponding bands in fig. 4. Therefore, these bridges serve as stress relievers near the boundary between crystalline and glassy phases.

Finally, the Raman spectrum of pure β-PbF_2 was presented in [15] and it consists of two very strong and narrow peaks at 190 and $240\,cm^{-1}$, which are apparently absent in our precursor glass and resulting glass-ceramic (fig. 4). This indicates that the total crystalline fraction in the glass-ceramic is below detection limit by Raman spectroscopy, *i.e.*, somewhere below 3 to 5% in volume.

REFERENCES

[1] Tikhomirov V. K., Furniss D., Seddon A. B., Ferrari M. and Rolli R., *J. Mater. Sci. Lett.*, **21** (2002) 293.
[2] Tikhomirov V. K., Furniss D., Seddon A. B., Reaney I. M., Beggiora M., Ferrari M., Montagna M. and Rolli R., *Appl. Phys. Lett.*, **81** (2002) 1937.
[3] Almeida R. M., *J. Non-Cryst. Solids*, **106** (1988) 347.
[4] Galeener F. L., Leadbetter A. J. and Stringfellow M. W., *Phys. Rev. B*, **27** (1983) 1052.

[5] McMillan P., *Amer. Mineral.*, **69** (1984) 622; McMillan P. and Piriou B., *J. Non-Cryst. Solids*, **55** (1983) 221; You J., Jiang J. and Xu K., *J. Non-Cryst. Solids*, **282** (2001) 125.
[6] Almeida R. M., Pereira J. C. and Alcala R., *Phys. Chem. Glasses*, **33** (1992) 187.
[7] Almeida R. M., *Fluoride Glasses*, in *Handbook on the Physics and Chemistry of Rare-earths*, edited by Gschneidner K. A. jr. and Eyring L., Vol. **15** (Elsevier) 1991, pp. 287-346.
[8] Duval E., Boukenter A. and Champagnon B., *Phys. Rev. Lett.*, **56** (1986) 2052.
[9] Montagna M. and Dusi R., *Phys. Rev. B*, **52** (1995) 10080; Ferrari M., Gonella F., Montagna M. and Tosello C., *J. Appl. Phys.*, **79** (1996) 2055.
[10] Kukkonen L. L., Reaney I. M., Furniss D. and Seddon A. B., *Phys. Chem. Glasses*, **42** (2001) 265.
[11] Manasreh M. O. and Pederson D. O., *Phys. Rev. B*, **30** (1984) 3482.
[12] Chuvaeva T. I., Dymshits O. S., Petrov V. I., Tsenter M. Y., Shashkin A. V., Zhilin A. A. and Golubkov V. V., *J. Non-Cryst. Solids*, **282** (2001) 306.
[13] Tikhomirov V. K., Santos L. F., Almeida R. M., Jha A., Kobelke J. and Scheffler M., *J. Non-Cryst. Solids*, **284** (2001) 198.
[14] Tikhomirov V. K., Jha A., Perakis A., Sarantopoulou E., Naftaly M., Krasteva V. and Seddon A. B., *J. Non-Cryst. Solids*, **256&257** (1999) 89.
[15] Kawamoto Y., Kanno R. and Qiu J., *J. Mater. Sci.*, **33** (1998) 63.